Transport in Deformable Hygroscopic Porous Media During Microwave Puffing

Vineet Rakesh and Ashim K. Datta
Dept. of Biological and Environmental Engineering, Cornell University, Ithaca, NY 14853

DOI 10.1002/aic.13793
Published online March 30, 2012 in Wiley Online Library (wileyonlinelibrary.com).

Microwave puffing is a process used to obtain low-fat healthy foods by rapid heating of food products to develop high internal pressures in the material that cause significant structural changes. Two-way coupling of complex multiphase transport and large deformations in the material, which is critical to simulate the puffing process accurately, was implemented. A porous media model that includes different phases, solid, liquid water, and gas, and incorporates pressure driven flow and evaporation was used to describe the transport processes in the material. Large deformations were included to model structural changes, with the material treated as hyperelastic. Arbitrary Lagrangian–Eulerian (ALE) framework was used. The model was validated using experimental temperature, moisture, and volume measurement and used to comprehensively understand the puffing process. Uncertainty analysis was carried out to estimate uncertainty in model prediction due to the choice of critical input parameters such as bulk modulus and permeabilities. © 2012 American Institute of Chemical Engineers *AIChE J,* 59: 33–45, 2013
Keywords: microwave puffing, large deformation, porous media, finite element method, multiphase flow, hyperelastic

Introduction and Objectives

In food processing, puffing is the rapid heating of food products to form vapor (and thus generate pressure) inside the material that in turn changes the food structure. Increased interest in the process is due to its ability to obtain low-fat healthy foods and ready-to-eat products that emulate some of the mechanical properties of deep fried foods.[1–3] Microwaves provide an excellent means to perform puffing because of the high internal heating rates involved. During the puffing process, the material is subjected to rapid heating using microwaves that leads to evaporation and pressure generation. This pressure build-up in turn causes the material to puff. The volume change in materials during processes such as potato puffing can be approximately[4] 15–25%. To develop and optimize this complex process, a comprehensive understanding of the process through physics-based modeling and experimentation is needed. Additionally, the physics of the problem is very similar to the general class of problems involving coupled multiphase transport and deformation in porous media relevant to various disciplines such as oil–gas flow in rocks,[5] ground water transport,[6] and biomedical applications.[7] The developed model can, therefore, be used to understand and optimize these important processes as well.

Microwave puffing is definitely a process with rapid heat and mass transfer combined with large deformations.[1,8] Although studies have been reported that aim to determine optimum processing conditions[4,9–12] by measuring properties[13–16] of fruits and vegetables for different puffing methods, attempts to understand the process comprehensively with the help of physics-based models are lacking with one exception in the case of vapor-induced puffing.[17] However, this particular work involves modeling bubble expansion in the pores in molten starch and does not consider the overall solid structure of the material that is critical and is intended in this work. Also, the model[17] is defined at a microscopic level and, therefore, does not include transfer of heat and water vapor in the continuum. Similarly, others have used bubble growth models for different applications.[18,19] Some others[20,21] have also used bubble growth models for studying extrusion and included transport of water vapor; however, these models used the effective diffusivity formulation, which does not provide insight into the transport phenomena, especially pressure driven flow and evaporation/condensation.

To model the microwave puffing process accurately, two-way coupling effects of transport and large deformation need to be considered. The transport problem itself is very complex due to the presence of multiple phases—solid, liquid (water), and gas (air and water vapor)—and multiple modes of transport—capillary flow, binary diffusion, and pressure driven flow—along with rapid phase change (evaporation/condensation). Researchers have implemented the transport problem with all the different components for various applications,[22–26] but they neglected any deformation. Some have only considered heat transfer with small[27] or finite deformations.[28] Others have implemented relatively simple transport problems coupled with small deformation models that do not account for all the different phenomena mentioned above.[29–31]

In case of microwave puffing, the solid mechanics problem becomes complex as well due to both geometric and

Correspondence concerning this article should be addressed to A. K. Datta at akd1@cornell.edu.

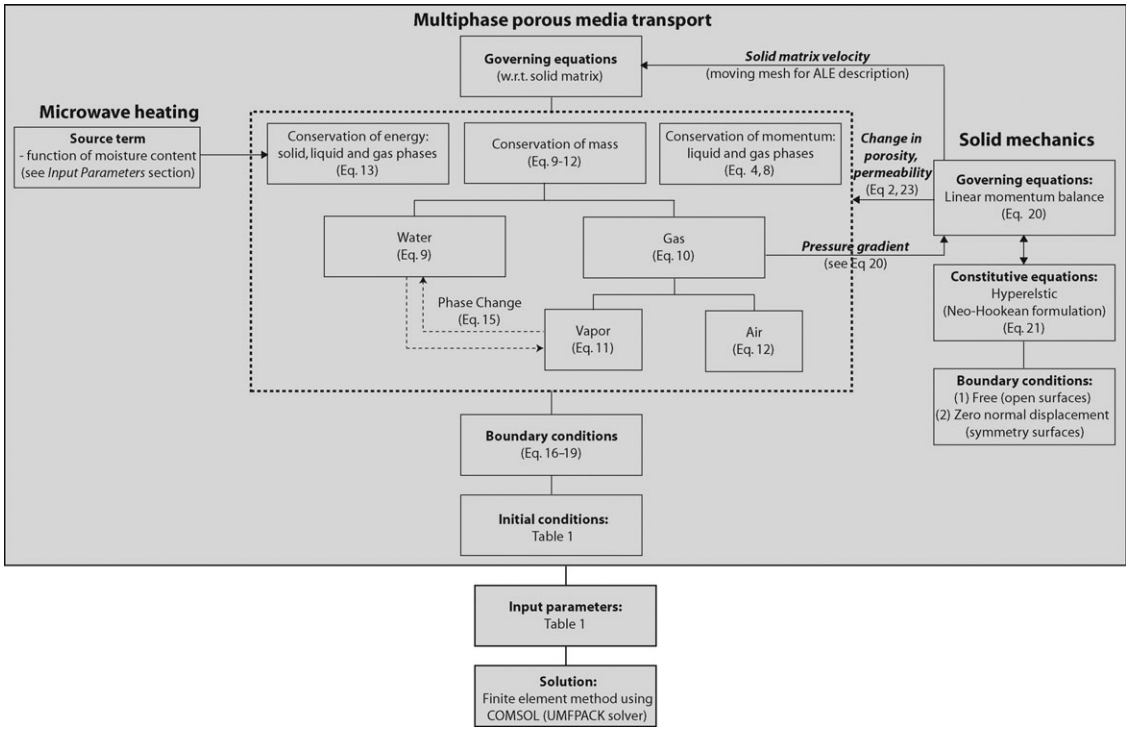

Figure 1. Flow chart showing the coupling between the different physics and the solution methodology.

material nonlinearity. The structural changes in the material are large, and hence, large deformations have to be considered. Most of the modeling work that have included detailed transport formulation have only implemented the small deformation version of the problem[32–35] in which the undeformed and deformed configurations of the material are considered to be the same. This assumption makes the model formulation simpler, but it cannot be applied to a process such as puffing where deformations are large, and one of the main objectives of modeling is to determine the deformation. Moreover, some of this work[32,33] use Luikov-type models where the transport cannot be easily related to measurable physical processes. Some others have included empirical models for deformations.[36] Other researchers[37–40] have considered large deformations, but their transport problem was not as complex with no phase change or hygroscopicity of the material. Yet others have included detailed transport but used linear constitutive relationships for large deformation problems,[5,41] which makes their models inconsistent. In this work, we not only implement multiphase transport in a porous material but also consider large deformations for the solid mechanics problem using a consistent hyperplastic (nonlinear) formulation. Although excellent texts exist that discuss similar problems especially in groundwater flow applications,[6,42,43] in our knowledge this complete problem with all the transport and solid mechanics components has not been solved.

Mathematical Model

As discussed earlier, the two-way coupling of multiphase porous media transport and solid mechanics (including large deformations) is critical to accurately simulate the microwave puffing process. The coupling is implemented by formulating the set of equations in a moving Arbitrary Lagrangian–Eulerian (ALE) grid setting.[37,44,45] The models for transport and solid mechanics and their coupling are discussed in detail in the following sections. The coupling is also shown schematically in Figure 1.

Transport-multiphase porous media model

A multiphase porous media model was formulated to describe the heat, mass, and momentum transport during microwave puffing. The sample was considered porous[46] with three phases: solid, liquid water, and gas. The gas phase had two components: water vapor and air. The schematic of a representative elementary volume (REV) of the material is shown in Figure 2a. The volume fraction of pores in a REV of the material, ΔV, at any time t is denoted by porosity, ϕ

$$\phi = \frac{\Delta V_{\mathrm{p}}}{\Delta V} = \frac{\Delta V_{\mathrm{w}} + \Delta V_{\mathrm{g}}}{\Delta V} \tag{1}$$

where ΔV_{w} and ΔV_{g} are the volume occupied by liquid water and gas phases in the REV, respectively. Note that this definition of porosity is generally what is considered in the porous media literature[46] and it includes the volume fraction of the gas as well as the liquid phase (water). This definition is different from the conventional meaning of porosity that only refers to gas phase volume fraction.

As the structure of the sample matrix changes due to deformation, the porosity changes. The volume of the solid matrix, however, does not change. Therefore, the porosity, ϕ, at any time t in a deforming medium can be determined using the following relation

$$(1 - \phi)\Delta V = (1 - \phi_0)\Delta V_0 \tag{2}$$

where ΔV_0 and ϕ_0 are the initial volume and porosity of a REV, respectively.

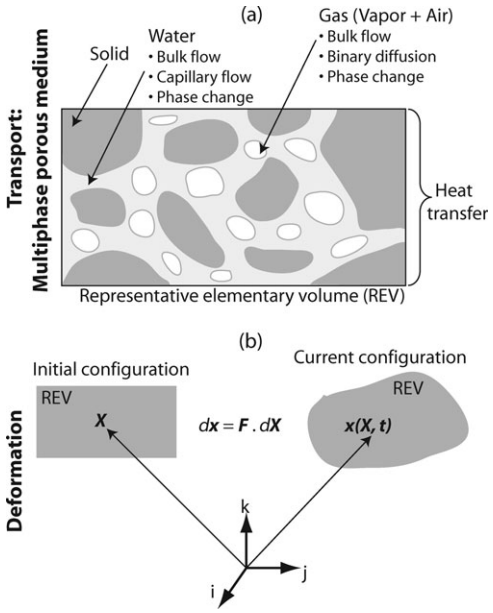

Figure 2. (a) REV of the porous medium with the different phases and modes of transport considered; (b) the initial and current configuration of a REV during deformation.

Here F is the deformation gradient tensor.

Momentum Balance. Darcy's law is considered for the flow of the movable phases (liquid water and gas) in the porous medium. For the deforming medium, the superficial velocity for each moving phase due to the gas pressure gradient in the medium, with respect to the solid matrix velocity, $\mathbf{v}_s$, is therefore given by

$$\mathbf{v}_{\mathrm{sup,i\,s}} = -\frac{k_i k_{r,i}}{\mu_i}\nabla P \tag{3}$$

where $i = w$ denotes the liquid water phase and $i = g$ the gas phase. Here, the relative velocity, $\mathbf{v}_{\mathrm{sup,i\,s}}$, is defined as $\mathbf{v}_{\mathrm{sup,i\,s}} = \mathbf{v}_{\mathrm{sup,i}} - \mathbf{v}_s$, and the total gas pressure is the sum of the partial pressures of vapor and air based on the ideal gas law, $P = p_a + p_v$. The relative velocity (with respect to the solid matrix) due to the gas pressure for each phase based on the volume occupied by that particular phase, is therefore, given by

$$\mathbf{v}_{i\,s} = -\frac{1}{S_i\phi}\frac{k_i k_{r,i}}{\mu_i}\nabla P \tag{4}$$

where S_w and S_g are the liquid water saturation and gas saturation, respectively. The saturations, S_i, denote the volume fraction of the liquid or gas phase with respect to pore volume

$$S_i = \frac{\Delta V_i}{\Delta V_p} = \frac{\Delta V_i}{\phi \Delta V} \tag{5}$$

Liquid water in the pores experiences capillary pressure, p_c, in addition to the gas pressure. Therefore

$$p_w = P - p_c \tag{6}$$

The effective velocity of the liquid phase (with respect to the solid matrix) is therefore given by

$$\begin{aligned}\mathbf{v}_{\mathrm{eff,w\,s}} &= -\frac{1}{S_w\phi}\frac{k_w k_{r,w}}{\mu_w}\nabla p_w \\ &= -\frac{1}{S_w\phi}\frac{k_w k_{r,w}}{\mu_w}\nabla P + \frac{1}{S_w\phi}\frac{k_w k_{r,w}}{\mu_w}\nabla p_c \\ &= \mathbf{v}_{w\,s} + \frac{1}{S_w\phi}\frac{k_w k_{r,w}}{\mu_w}\frac{\partial p_c}{\partial S_w}\nabla S_w\end{aligned} \tag{7}$$

Equation 7 can be rewritten in terms of capillary diffusivity,[47] $D_c = -\frac{k_w k_{r,w}}{\phi\mu_w}\frac{\partial p_c}{\partial S_w}$, and water concentration, $c_w = \rho_w \phi S_w$

$$\mathbf{v}_{\mathrm{eff,w\,s}} = \mathbf{v}_{w\,s} - \frac{D_c}{c_w}\nabla c_w \tag{8}$$

Mass Balance. The mass balance equation for the transportable phases includes the effects of bulk flow (convection), binary diffusion (gas phase), and capillary flow (liquid phase). Mass conservation equation for the liquid water phase includes the bulk flow, capillary flow, and phase change. The equation is written using the ALE description with the mesh moving with the solid matrix velocity $\mathbf{v}_s$[5]

$$\frac{\partial c_w}{\partial t} + (\mathbf{v}_w - \mathbf{v}_s)\cdot\nabla c_w + c_w\nabla\cdot\mathbf{v}_w = \nabla\cdot(D_c\nabla c_w) - \dot{I} \tag{9}$$

Similarly, the continuity equation for the gas phase is given by

$$\frac{\partial c_g}{\partial t} + (\mathbf{v}_g - \mathbf{v}_s)\cdot\nabla c_g + c_g\nabla\cdot\mathbf{v}_g = \dot{I} \tag{10}$$

Mass balance equation for the vapor component of the gas phase includes bulk flow, binary diffusion, and phase change

$$\frac{\partial c_v}{\partial t} + (\mathbf{v}_g - \mathbf{v}_s)\cdot\nabla c_g + c_g\nabla\cdot\mathbf{v}_g = \nabla\cdot\left(S_g\phi\frac{C^2}{\rho_g}M_a M_v D_{\mathrm{eff,g}}\nabla x_v\right) + \dot{I} \tag{11}$$

Here, vapor concentration is related to the gas concentration by its mass fraction, $c_v = \omega_v c_g$. Similarly, concentration of air, c_a, is $\omega_a c_g$. The mass fraction of air can be calculated using the mass fraction of vapor from Eq. 11

$$\omega_a = 1 - \omega_v \tag{12}$$

Energy Balance. The energy balance equation is solved for the mixture, and the effect of microwave heating is included as a source term. Detailed discussion regarding microwave source term calculation is included in the "Input Parameters" section. Energy conservation includes convection due to moving phases, conduction, phase change and microwave power absorption term

$$\begin{aligned}&\left[\sum_{i=s,w,v,a}(c_i c_{p,i})\right]\frac{\partial T}{\partial t} + \sum_{i=w,v,a}(\mathbf{v}_i - \mathbf{v}_s)\cdot\nabla(c_i c_{p,i}T) \\ &\quad + \sum_{i=w,v,a}(c_i c_{p,i}T\,\nabla\cdot\mathbf{v}_i) - c_{p,w}T\,\nabla\cdot(D_c\nabla c_w) \\ &\qquad = \nabla\cdot(k_{\mathrm{eff}}\nabla T) - \lambda\dot{I} + Q_{\mathrm{mic}}\end{aligned} \tag{13}$$

Here, the effective thermal conductivity is given by the volume weighted average of the different phases and components

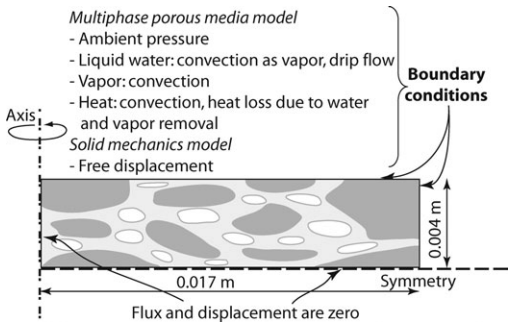

Figure 3. Schematic and boundary conditions for the problem.

$$k_{\text{eff}} = (1-\phi)k_{\text{s}}^{\text{th}} + \phi\left\{S_{\text{w}}k_{\text{w}}^{\text{th}} + S_{\text{g}}\left(\omega_{\text{v}}k_{\text{v}}^{\text{th}} + \omega_{\text{a}}k_{\text{a}}^{\text{th}}\right)\right\} \quad (14)$$

Evaporation/Condensation. The porous media model incorporates the change of phase between liquid water and vapor (evaporation/ condensation) throughout the domain using the following expression[22]

$$\dot{I} = K_{\text{evap}}\frac{M_{\text{v}}}{RT}\left(p_{\text{v,eq}} - p_{\text{v}}\right) \quad (15)$$

where $p_{\text{v,eq}}$ is the equilibrium vapor pressure, which is a function of both temperature and moisture content of the material.

Boundary Conditions. The boundary conditions for the transport problem are now listed and are also shown in Figure 3. Pressure was set to ambient at the open surfaces (top and right boundaries in Figure 3) for solving Eq. 10

$$P|_{\text{s}} = P_{\text{amb}} \quad (16)$$

Water from the interior can move out of the boundary as vapor after evaporation. When the liquid water saturation becomes high ($S_{\text{w}} = 1$), water can also move out of the open surfaces directly by drip flow. Therefore, the boundary condition for Eq. 9 was set as

$$j_{\text{n,w}}|_{\text{s}} = h_{\text{m}}\phi S_{\text{w}}\left(\rho_{\text{v}} - \rho_{\text{v, oven}}\right) + \underbrace{c_{\text{w}}v_{\text{n,w}}}_{\text{when } S_{\text{w}}=1} \quad (17)$$

where $j_{\text{n,w}}$ is the total normal flux of water at a particular surface. Vapor can be convected away from the open surfaces. Therefore, the following was set as the boundary condition for Eq. 11

$$j_{\text{n,v}}|_{\text{s}} = h_{\text{m}}\phi S_{\text{g}}\left(\rho_{\text{v}} - \rho_{\text{v, oven}}\right) \quad (18)$$

The air inside the microwave is at room temperature; therefore, the surface of the sample is subjected to cooling by convection. The loss of heat due to evaporation of water, removal of liquid water (during drip flow), and vapor is also included in the boundary condition for heat transfer (Eq. 13)

$$q_{\text{n}}|_{\text{s}} = h(T - T_{\text{amb}}) - h_{\text{m}}\phi S_{\text{w}}\left(\rho_{\text{v}} - \rho_{\text{v, oven}}\right)\lambda - h_{\text{m}}\phi\left(S_{\text{w}} + S_{\text{g}}\right)\left(\rho_{\text{v}} - \rho_{\text{v, oven}}\right)c_{\text{p,v}}T - \underbrace{c_{\text{w}}v_{\text{n,w}}\,c_{\text{p,w}}T}_{\text{when } S_{\text{w}}=1} \quad (19)$$

where q_{n} is normal heat flux.

Initial Conditions. The initial conditions for the different variables are listed in the input parameters (Table 1).

Solid Mechanics

To determine the deformation in the material during the puffing process, an appropriate solid mechanics model[55] needs to be formulated and solved. The model should include geometric as well as material nonlinearity.[56] Large deformations in the REV and the deformation gradient tensor for the mapping are illustrated in Figure 2b.

Linear Momentum Balance. The linear momentum balance is solved to obtain the stresses. As large deformations are involved, Lagrangian measures of stress and strain are used.[44] The gas pressure gradient causes the deformation. Therefore

$$\nabla_X \cdot \left(\mathbf{S}\cdot\mathbf{F}^{\text{T}}\right) - \nabla P = 0 \quad (20)$$

where $\mathbf{S}$ is the second Piola–Kirchhoff (PK2) stress tensor, $\mathbf{F}$ is the deformation gradient tensor, and P is the gas pressure. Notation X refers to the Lagrangian reference frame. The PK2 stress is related to the Cauchy stress, which is normally used for small deformation problems, by[56]

$$\mathbf{S} = J\mathbf{F}^{-1}\cdot\sigma\cdot\mathbf{F}^{-T} \quad (21)$$

where J is the Jacobian determinant of the deformation gradient tensor, $\mathbf{F}$. The strain measure is the Green–Lagrange (or Green) strain tensor, $\mathbf{E}$, given by[56]

$$\mathbf{E} = \frac{1}{2}\left(\mathbf{F}^{\text{T}}\cdot\mathbf{F} - \mathbf{I}\right) \quad (22)$$

The stored energy function, W, relates the stress and strain tensors[44]

$$\mathbf{S} = \frac{\partial W}{\partial \mathbf{E}} \quad (23)$$

To solve Eq. 20, we need to consider an appropriate material model (constitutive equations) and thereby determine the form of this stored energy function. This is now discussed.

Constitutive Equations. As discussed earlier, puffing involves large deformation of the material and therefore, a nonlinear material model (stress–strain relationship) needs to be used to obtain a consistent formulation for the problem. The linear Hooke's law of elasticity is applicable only for the special case of small deformations and is not valid in this case. The hyperelastic Neo-Hookean material model is an extension of the Hooke's law of elasticity to large deformations. Therefore, the Neo-Hookean formulation is considered for the problem. The stored energy function for a Neo-Hookean material is given by[44]

$$W = \frac{K}{2}(J-1)^2 - \frac{G}{2}\left(\bar{I}_1 - 3\right) \quad (24)$$

where K and G are the initial bulk and shear modulus, respectively. Here, $\bar{I}_1$ is the first invariant (trace) of the right Cauchy–Green tensor, $\overline{\mathbf{C}}$ ($= \overline{\mathbf{F}}^{\text{T}}\cdot\overline{\mathbf{F}}$), for the volume preserving (deviatoric) part. The first and second terms on the right-hand side of Eq. 24 are the volumetric and deviatoric contributions, respectively. The multiplicative split of the deformation gradient tensor into volumetric and deviatoric parts is defined by[56]

Table 1. Input Parameters for the Simulations

Parameter	Value	Source
Sample size (m)	0.034 (dia) × 0.008 (h)	
Viscosity		
Water, μ_w (Pa s)	0.988×10^{-3}	
Vapor and air, μ_g (Pa s)	1.8×10^{-5}	
Intrinsic permeability		
Water, k_w (m^2)	5×10^{-16}	Ref. 48
Vapor and air, k_g (m^2)	2×10^{-15}	Ref. 48
Relative permeability		
Water, $k_{r,w}$	$[(S_w - 0.09)/0.91]^3 f(\phi)$, $S_w > 0.09$; 0, $S_w < 0.09$	Ref. 46
Vapor and air, $k_{r,g}$	$[1–1.1S_w] f(\phi)$, $S_w < 1/1.1$; 0, $S_w > 1/1.1$	Ref. 46
Capillary diffusivity (water), D_c ($m^2\ s^{-1}$)	$4.5 \times 10^{-7} \exp(-2.8 + 2M)$	
Binary diffusivity, $D_{eff,g}$ ($m^2\ s^{-1}$)	2.6×10^{-5}	Ref. 48
Specific heat capacity (J $kg^{-1}\ K^{-1}$)		
Solid, c_{ps}	1650	Ref. 49
Water, c_{pw}	4178	Ref. 49
Vapor, c_{pv}	2062	Ref. 49
Air, c_{pa}	1006	Ref. 49
Thermal conductivity (W $m^{-1}\ K^{-1}$)		
Solid, k_s^{th}	0.21	Ref. 49
Water, k_w^{th}	0.57	Ref. 49
Vapor, k_v^{th}	0.026	Ref. 49
Air, k_a^{th}	0.026	Ref. 49
Density (kg m^{-3})		
Solid, ρ_s	1530	
Water, ρ_w	998	
Vapor, ρ_v	Ideal gas law	
Air, ρ_a	Ideal gas law	
Latent heat of vaporization, λ (J kg^{-1})	2.26×10^6	
Evaporation rate constant, K (s^{-1})	1×10^{-3}	Ref. 22
Equilibrium vapor pressure, $p_{v,eq}$ (Pa)	$p_{sat}(T) \exp(-0.0267M^{-1.656} + 0.0107e^{-1.287M} M^{1.513} \ln[p_{sat}(T)])$	Ref. 50
Ambient pressure, P_{amb} (Pa)	101,325	
Mass transfer coefficient, h_m (m s^{-1})	0.011	Ref. 23
Heat transfer coefficient, h (W $m^{-2}\ K^{-1}$)	20	Ref. 23
Ambient temperature, T_{amb} (°C)	22	
Microwave source term, Q_{mic} (W m^{-3})	$1.5 \times 10^7\ [M_0/M]^{-1.17}$	
Bulk modulus, K (Pa)	4.594×10^5	Ref. 51 and 52
Shear modulus, G (Pa)	7.94×10^4	Ref. 53
Initial Conditions		
Porosity, ϕ_0	0.80	Ref. 54
Pressure, P_0 (Pa)	101,325	
Water concentration, $c_{w,0}$ (kg m^{-3})	459	
Vapor mass fraction, $\omega_{v,0}$	0.01	
Temperature, T_0 (°C)	22	

$$\mathbf{F} = J^{\frac{1}{3}}\,\overline{\mathbf{F}} \tag{25}$$

where $J^{\frac{1}{3}}$ is the volumetric part, and $\overline{\mathbf{F}}$ is the volume preserving part. By definition, the Jacobian determinant of the deformation gradient tensor for the volume preserving part should be unity, which can be confirmed from Eq. 25. It can be observed that the multiplicative split for the large deformation case is analogous to the case of small deformation where an additive split of the volumetric and deviatoric parts is used ($\varepsilon = \mathbf{e} + 1/3\ \mathrm{tr}[\varepsilon]\mathbf{I}$). Finally, the deformation causes change in porosity, which is given by Eq. 2.

Boundary Conditions. The normal displacements on the symmetry boundaries to set to zero (see Figure 3). The other boundaries have no constraints and are free to move.

Input parameters

All input parameters used for the simulations are listed in Table 1. Some of the input parameters are discussed here.

Porosity Factor for Water and Gas Permeability. The porosity of material (as defined by Eq. 1) changes with deformation as given by Eq. 2. With change in porosity of the material, liquid and gas permeabilities also change. The porosity factor, $f(\phi)$, in the Kozeny–Carman equation relates the liquid and gas permeability to the porosity.[46] It is given by

$$f(\phi) = \left(\frac{\phi}{\phi_0}\right)^3 \left(\frac{1-\phi_0}{1-\phi}\right)^2 \tag{26}$$

The liquid and gas permeability values were multiplied by this factor to include the effect of porosity change on permeability in the model.

Bulk Modulus. From literature,[51] the bulk modulus of raw uncooked potato was found to be 5 MPa. However, the same work[51] acknowledged that the modulus would decrease as the cell walls degrade during cooking or heating causing softening of potato samples. Others[52,53,57,58] have also shown that different processing conditions such as drying and microwave heating change the mechanical properties (e.g., Young's modulus) of raw potatoes substantially. They, however, did not measure the bulk modulus or the Poisson's ratio. In comparing boiling and microwave heating of potatoes,[52] microwave heating was shown to result in more significant changes in mechanical properties of raw potato due

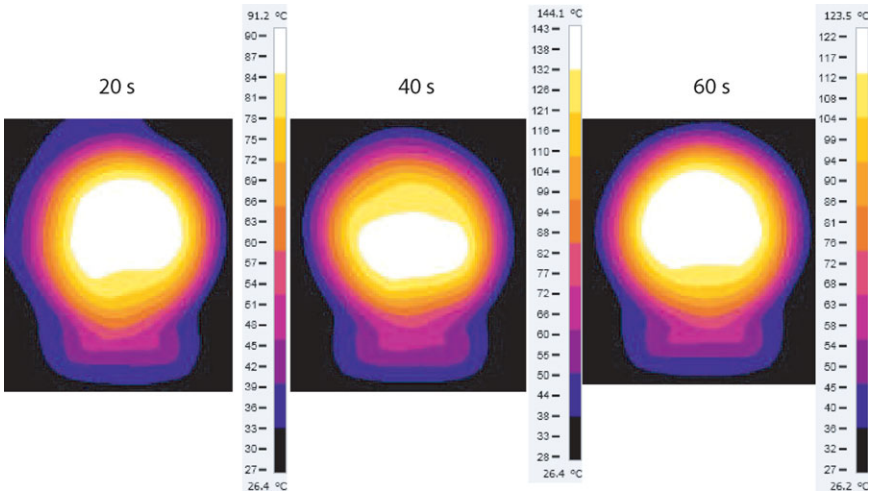

Figure 4. Spatial temperature distribution on the top surface of the samples as obtained from the thermal imaging camera after different times during puffing.

[Color figure can be viewed in the online issue, which is available at wileyonlinelibrary.com.]

to advanced changes in the microstructure of potato tubers, and breakdown of hemicellulose and cellulose components with changes in cell appearance that can include cell separation. Their data showed a 91% decrease in mechanical properties during microwave heating as compared to the raw state. Based on the bulk modulus value of raw potatoes undergoing microwave heating, a bulk modulus of 459.4 kPa was used for this study.

Shear Modulus. A shear modulus value of 79.4 kPa was obtained from the literature[53] for microwave-heated potatoes.

Microwave Source Term. As the sample size is very thin (Table 1), a uniform microwave power absorption can be assumed in the sample initially. The initial power was measured using the IMPI 2l test.[59] The power was scaled to account for the lower volume of the sample using data for power absorbed as function of sample volume from the literature.[60] At later times, the microwave power was a function of moisture content and the relation (listed in Table 1) was also obtained from the published literature.[23]

Solution details

As the sample was cylindrical, a 2-D axisymmetric geometry was considered, as shown in Figure 3, to reduce computational requirements. The governing equations were solved in COMSOL Multiphysics 3.5a (COMSOL, Burlington, MA) using the UMFPACK direct solver with a maximum time step of 0.01 s. The Chemical Engineering and Structural Mechanics modules in COMSOL Multiphysics were used for the model. The procedure followed for solving the coupled problem is schematically illustrated in Figure 1. A tetrahedral mesh with 13,128 elements was used based on mesh convergence analysis (not shown here). The simulations were run on a 3-GHz Windows workstation running on Windows XP Professional 64 bit with 16-Gb memory.

Experimental Methodology

Potato samples were used to study the microwave puffing process experimentally. Cylindrical samples were obtained by cutting fresh Russet potatoes using a punch. The experimental methodology used in the literature for hot-air puffing of potatoes[4] was followed. The cylindrical samples were initially blanched for 2 min by placing them in boiling water. Blanching was performed to stop enzyme action and soften the samples. Drying was then carried out slowly at 90 °C for 80 min in a hot air oven (Thermador JetDirect oven, Model CJ302UB, Enersyst Development Center, Dallas, TX). The samples were dried to a low moisture content (~1.6–1.8 db), so that a partially impermeable layer was formed at the surface that would restrict escape of gases during puffing. Puffing was then performed by subjecting the samples to rapid heating using microwaves for 60 s. Point temperatures were measured as functions of heating time in the sample during the puffing process using a fiber optic system (Fiso Technologies, Quebec, Canada). Spatial distribution of temperature at the surface of the samples was obtained using an infrared thermal imaging camera (FLIR A320, FLIR Systems, Boston, MA). Moisture loss was determined as a function of time by puffing samples to different times and measuring the weight loss (Ohaus Voyager Pro Balances VP64CN, Ohaus Corporation, Pine Brook, NJ; 0.1 mg least count). The change in volume of the samples during puffing was measured using the rapeseed displacement method[61] with a resolution of 0.5 cm^3. Three replicates were taken for each measurement.

Results and Discussion

Validation of the model was done by comparing the computed results with the experimental measurements of temperature and moisture loss histories and volume change. Transient and spatial temperature, moisture, pressure, evaporation rate, and porosity during the puffing process are discussed, followed by sensitivity analysis of the model to critical input parameters.

Experimental validation

Spatial Temperature Distribution at the Sample Surface. The spatial temperature profiles at the sample surface at different times during puffing obtained from infrared thermal imaging is shown in Figure 4. It must be noted here that the cross-sections do not appear circular, because the heated air around the circular samples is also included in the thermal camera image. Very high temperatures are observed after 60 s of puffing. In 60 s, most of the moisture is released in the form of liquid water due to drip flow and as water vapor.

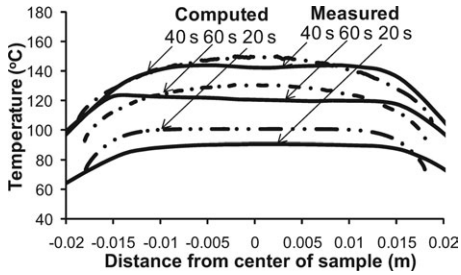

Figure 5. Computed and measured (using thermal imaging camera) temperature distribution at the top surface of the samples at different times.

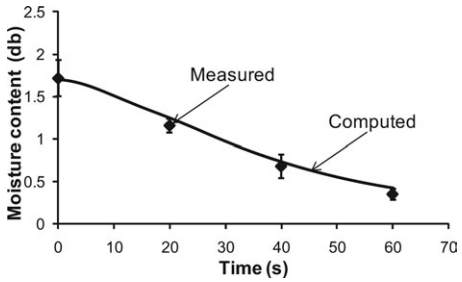

Figure 7. Computed and measured (determined from weight loss) moisture content in the samples as a function of puffing time (time since the start of microwave heating).

Error bars represent the standard deviation for three measurements.

The residual mass comprises mostly of the solid matrix whose temperatures become very high. The highest temperature is obtained after 40 s, and then, it starts to fall, as the microwave power absorption reduces because of moisture loss while cooling takes place at the surface. It can also be observed that the temperature contours are fairly symmetric in the axial direction; thereby justifying the use of an axisymmetric model to reduce computational requirements. These temperatures maps obtained from thermal imaging were then used to determine temperatures in the axial direction and were compared with the simulated results, as shown in Figure 5. The comparisons are seen to be quite good. The experimental temperatures are expected to be lower, because temperature measurement using the infrared camera was done after the puffing process and the time lag ($\sim$10 s) can lead to cooling.

Temperature History. To perform a more detailed validation, temperature histories were obtained from experiments at a region about 2 mm below the surface of the sample and halfway from the axis. This is shown in Figure 6. The location of this region is approximate, because it was nearly impossible to position the fiber optic probe exactly due to the small dimension of the sample and the finite thickness of the probe. In addition, the size of the sample changes considerably during the puffing process. The point temperature measurements, therefore, only provide a qualitative assessment of the temperature ranges that are observed during the puffing process. Three different measured temperature histories (using fresh samples) are shown in Figure 6 along with the predicted temperature history at the same location. The temperatures predicted by the model are found to be consistent with the measured values, that is, predictions are within the range of measured values.

Moisture Loss. As shown in Figure 7, total moisture contents obtained from the computational model as function of time was found to closely match those determined gravimetrically.

Volume Change. Figure 8 compares the volume changes predicted by the model with those measured experimentally. The general trend of volume change predicted by the model was found to match the experimental result. A more accurate determination of the solid mechanics parameters (bulk modulus and shear modulus) and increasing the accuracy of the volume measurement may lead to a better match. A detailed uncertainty analysis is presented later. The initial increase in volume with time, followed by a decrease, is attributed to the decrease in microwave absorption due to moisture loss. As a result, evaporation decreases, and there is less vapor formation leading to lower pressures in the domain. There is also a constant loss of vapor at the surface, which further decreases pressures in the domain and thereby the volume of the sample decreases. Maximum volume around the same time ($\sim$40 s) has also been reported earlier.[62]

Figure 9 shows the change in structure of the sample at different times during the puffing process along with the deformed mesh. There is considerable change in volume during the puffing process. From Figure 8, it can be observed that the final change is about 20%. It is consistent with a previous experimental study,[4] which also reported about

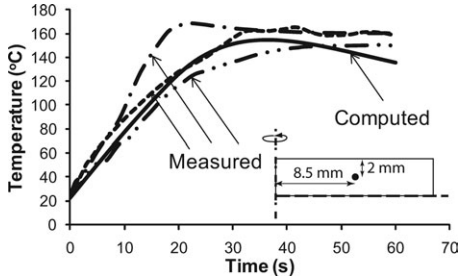

Figure 6. Computed and measured (using fiber optic probes) temperature history at a point 2 mm from the top surface and halfway from the axis of the sample (as shown).

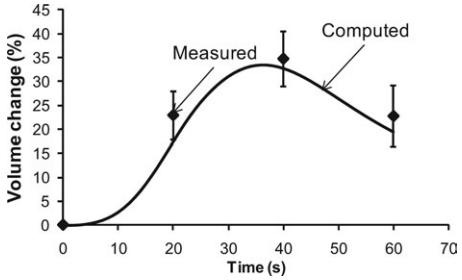

Figure 8. Computed and measured (determined using rapeseed displacement method) volume change in the samples as a function of puffing time (time since the start of microwave heating).

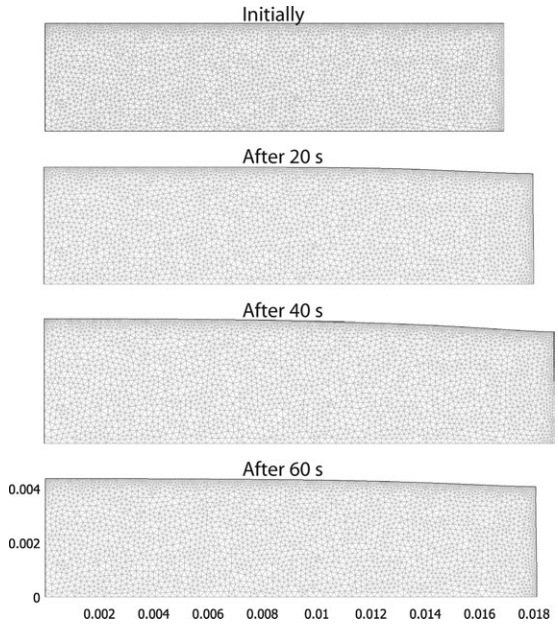

Figure 9. The deformed domain of the sample with the respective meshes at different times during the puffing process.

25% volume change for hot air puffing (at 200°C) of potatoes.

As could be expected, significant natural variability exists in the property values between potato samples. These could also lead to inconsistency in comparison of the computed and measured variables. However, based on the experimental comparisons of the three model parameters (temperature, moisture, and volume change), the model is considered to be validated. The analysis of the results is now presented along with sensitivity and uncertainty analysis.

Change in temperature, moisture, evaporation rate, pressure, and porosity during puffing

Temperature, moisture, evaporation rate, pressure, and porosity distribution in the domain at different times during puffing obtained from the simulation are shown in Figures 10–14. Temperatures in the interior of the sample increase with puffing time because of heating (from the microwaves), as shown in Figure 10. The sample surface is exposed to the air at room temperature, which cools the surface. The temperatures are, therefore, generally higher in the interior.

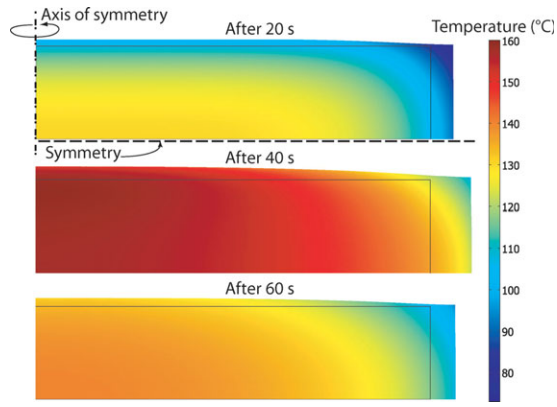

Figure 10. Computed temperature values inside the sample at different times during puffing.

The initial temperature of the sample was 22°C. The inner rectangle represents the initial dimensions before puffing. [Color figure can be viewed in the online issue, which is available at wileyonlinelibrary.com.]

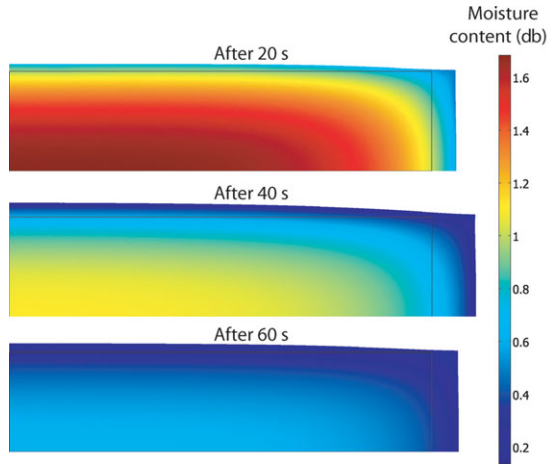

Figure 11. Computed moisture content inside the sample at different times during puffing.

The initial moisture content of the sample was 1.7 db. [Color figure can be viewed in the online issue, which is available at wileyonlinelibrary.com.]

Liquid water is transported inside the solid (a porous medium) by the capillary forces. Water is lost from the surface by evaporation to water vapor, and by drip flow when surface water saturation becomes close to unity. As temperature increases because of rapid heating, liquid water also evaporates over the whole domain (Figure 12) forming water vapor that moves more readily to the surface from where it is convected away. The surface moisture content (Figure 11) is, therefore, found to be very low as a result of these loses. With time, considerable moisture is lost throughout the domain (from 1.7 to 0.4 db) as shown in Figure 11.

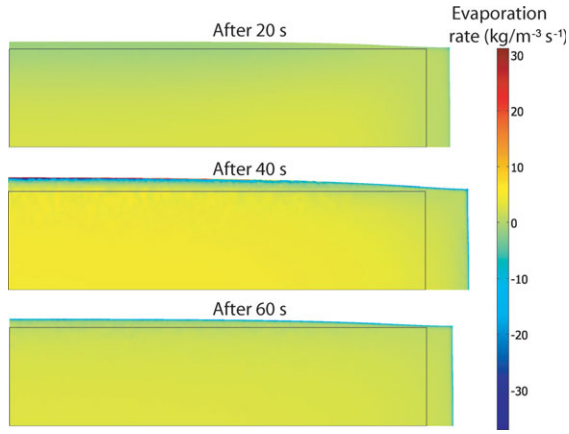

Figure 12. Computed evaporation rates inside the sample at different times during puffing.

Positive values represent evaporation, and negative values correspond to condensation. Evaporation occurs over the whole domain. At the surface, due to lower surrounding temperatures, some condensation is observed. [Color figure can be viewed in the online issue, which is available at wileyonlinelibrary.com.]

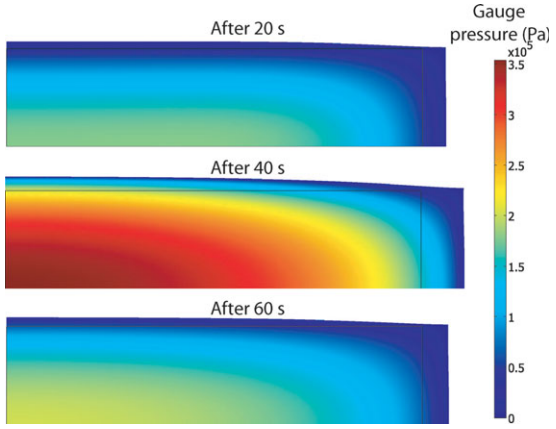

Figure 13. Computed gauge pressures inside the sample at different times during puffing.

Highest pressures occur near the center of the material. [Color figure can be viewed in the online issue, which is available at wileyonlinelibrary.com.]

As more liquid water evaporates into vapor, the pressure inside the medium increases. It can be seen from Figure 13 that significantly high pressures are developed. These high pressures cause the material to deform (shown in Figure 9). The porosity of the material (as defined by Eq. 1) in turn changes due to the deformation (Figure 14). The very large deformations lead to significant change in porosity of the material as given by Eq. 2. However, a feedback mechanism comes into play that prevents further increase in pressure. As porosity increases, there is a drastic increase in the permeability, as given by the Kozeny–Carman porosity factor (Eq. 26). Due to increase in the gas permeability, the pressure decreases at a particular location. The pressure, therefore, remains bounded, which may be one of the reasons that the material does not rupture during the process. It must also be noted that the vapor pressure in the porous medium is expected to be different compared to pure water, as the vapor pressure in the porous medium (potato sample) is not only a function of temperature but also a function of moisture content.[63,64] The relationship between vapor pressure and temperature and moisture content of the potato sample was obtained from the literature[50] and is shown in Table 1.

Sensitivity of the model to input parameters

With a large number of parameters needed in the complex model along with unavailability of accurate values for some of these parameters, it is necessary to quantify the model sensitivity to different parameters to have greater confidence in the predicted results. For example, the value of bulk modulus has not been measured for the material for the series of processes considered here, that is, blanching followed by slow drying followed by intensive microwave heating. To determine how these parameters affect the results, sensitivity analysis was done for three of the parameters whose accurate values were particularly difficult to find in existing literature–bulk modulus and permeabilities of water and gas. For bulk modulus, the chosen value (Table 1) was varied by $\pm 20\%$. Similarly, chosen permeability values (Table 1) were varied by $\pm 50\%$. Moisture content and volume change histories, the two most important parameters in a puffing process, were computed as affected by the variation in bulk modulus and permeability values.

Bulk Modulus. Four additional values of bulk modulus ($\pm 10\%$, $\pm 20\%$) were used to determine the sensitivity of the model to this parameter. The bulk modulus value for potatoes undergoing intensive heating processes was estimated based on the literature data on uncooked potato as discussed in detail in the "Input Parameters" section earlier. The range of bulk modulus values for sensitivity analysis was obtained using data for uncooked potatoes from four different sources.[52,53,57,58] Moisture loss and volume change histories for the different bulk modulus values used in simulations are plotted in Figure 15. The change in bulk modulus values does not significantly affect the moisture loss predicted from the model, as can be seen in Figure 15a. The volume change, however, depends considerably on the value of bulk modulus. Lower values of bulk modulus represent softened tissues that are easier to deform, and therefore, the volume increase is the greatest for the smallest value of bulk modulus (at -20 of the original value). Deformation in the material causes change in porosity that can potentially affect the transport processes inside the medium (e.g., Eq. 26). However, the changes in porosity are insignificant here, with change of 0.44 and -0.33% for -20% and 20% increase in bulk modulus values, respectively. As a result, transport inside the medium remains independent of the change in the bulk modulus value, which would explain the lack of sensitivity of moisture loss to bulk modulus. This lack of sensitivity can also imply a reduced need for obtaining more accurate values of bulk modulus through experimentation for predicting moisture loss. It must, however, be noted that volume change is dependent on the bulk modulus value chosen. To summarize, the choice of bulk modulus value influences the deformation part of the model more than the transport processes.

Water and Gas Permeability. Measurement of permeabilities of biological materials is still not a standard technique, and literature shows a wide range of liquid and gas permeability values in potatoes.[23,48,65] The reported values vary by more than two orders of magnitude, and these variations are so large that it is not feasible to incorporate them in the sensitivity analysis study, as they render the problem nonphysical (without corresponding change in other property values

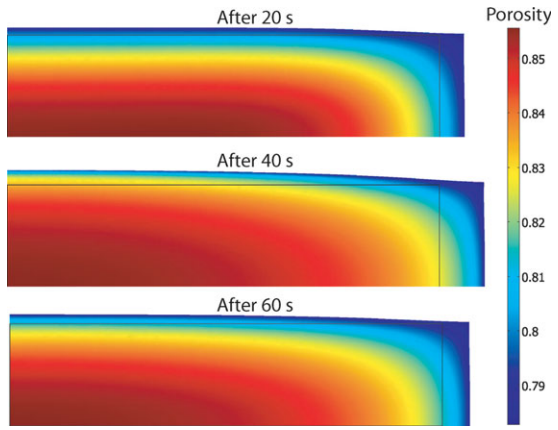

Figure 14. Computed change in porosity of the samples at different times during puffing.

The initial porosity of the sample was 0.8. Note that this porosity only represents the change in volume of the material, and it does not represent the loss of water. [Color figure can be viewed in the online issue, which is available at wileyonlinelibrary.com.]

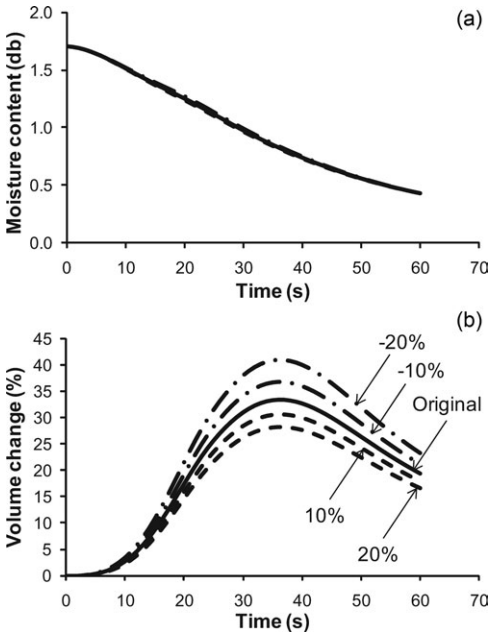

Figure 15. (a) Sensitivity of the process to change in bulk modulus using the total moisture loss as the variable of interest.

The moisture loss history is plotted for five different values of bulk modulus: the original value (given in Table 1) and 10, 20, −10 and −20% of the original value. (b) Sensitivity to the bulk modulus value with total volume change as the variable.

with parameters such as moisture content and porosity). To include a large variation, water and gas permeability values were considered in range of ±50% of the original value. The resulting change in moisture content and volume change of the material are plotted in Figure 16. Similar to the change in bulk modulus values, it is found that the change in permeability values did not affect the total moisture loss as much, but the volume change was influenced considerably. This is due to the drastic change in pressures inside the domain with change in permeability values. When gas permeability decreases, there is additional resistance to flow through the porous media (as given by Eq. 3) and as a result, the pressures increase.

Uncertainty Analysis. An uncertainty analysis, following the work of Rabin,[66] is performed for estimating the uncertainty in volume prediction from the model due to simultaneous variation in bulk modulus and permeability. Keeping all other parameters fixed, the volume at a specific time can be a function of bulk modulus (K) and permeability (k)

$$V = f(K, k) \tag{27}$$

Here, the effect of both liquid and gas permeability is lumped into the variable k. The uncertainty in volume is, therefore

$$V \pm \Delta V = f(K \pm \Delta K, k \pm \Delta k) \tag{28}$$

where Δ is the uncertainty interval for the two parameters. Using a first-order approximation, we get

$$V \pm \Delta V = f \pm \frac{\partial f}{\partial K}\Delta K \pm \frac{\partial f}{\partial k}\Delta k \tag{29}$$

To include the combined effect of all the uncertainties and to avoid inconsistencies due to plus or minus sign in the different uncertainties, a statistical approach is taken.[67] The total uncertainty is, therefore, defined as the square root of the sum of the errors squared

$$\Delta V = \sqrt{\left(\frac{\partial f}{\partial K}\Delta K\right)^2 + \left(\frac{\partial f}{\partial k}\Delta k\right)^2} \tag{30}$$

The partial derivatives are estimated using a central differencing scheme, that is, the derivatives are calculated using function values corresponding to the maximum and minimum values of the particular parameter. For example, for bulk modulus values

$$\Delta V_K = \frac{\partial f}{\partial K}\Delta K \approx \frac{V_{K,\max} - V_{K,\min}}{2} \tag{31}$$

The percentage uncertainties plotted in Figure 17 are, therefore, defined as

$$\Delta V_{\text{mod}} = \frac{\Delta V_{\text{K}}}{V_{\text{org}}} \times 100, \quad \Delta V_{\text{perm}} = \frac{\Delta V_{\text{k}}}{V_{\text{org}}} \times 100, \quad \Delta V_{\text{overall}} = \frac{\Delta V}{V_{\text{org}}} \times 100 \tag{32}$$

The overall uncertainty, in general, keeps increasing with the process time (Figure 17) reaching a maximum value of about 9% after 46 s. Uncertainty in the choice of permeability values affect the volume change more than the uncertainty in the bulk modulus value chosen. The effects of independent change in these parameter values on the model predictions has been discussed in detail in the previous section. The results from this uncertainty analysis basically show that there may be large uncertainties in the volume change predicted by the model

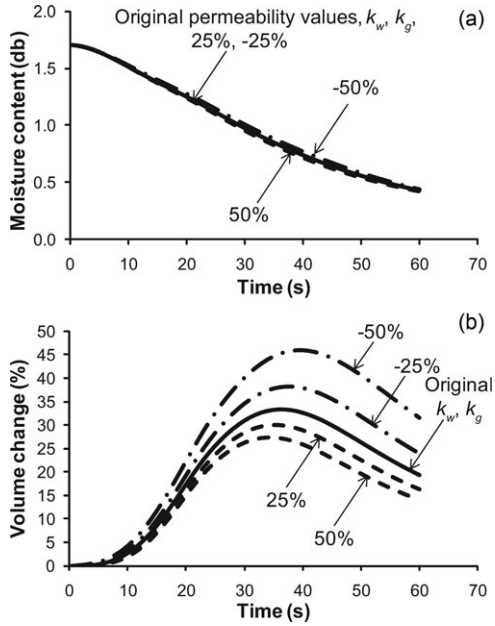

Figure 16. (a) Sensitivity of the process to change in liquid and gas permeabilities using the total moisture loss as the variable of interest.

The moisture loss history is plotted for five different sets of permeabilities: the original set (k_w and k_g values given in Table 1) and 25, 50, −25 and −50% of the original set of values. (b) Sensitivity of total volume change to liquid and gas permeabilities.

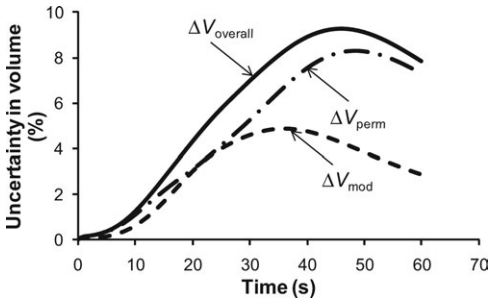

Figure 17. Uncertainty in volume change prediction from the model with time due to the variation in bulk modulus (±20% change) and permeability values (±50% change).

The quantities ΔV_{mod}, ΔV_{perm} and $\Delta V_{overall}$ represent uncertainty due to variation in bulk modulus only, permeability only, and simultaneous variation in bulk modulus and permeability, respectively.

depending on the chosen input parameter values. Accordingly, in general, uncertainty in the predictions must be considered while comparison with experimental data, for example, in the volume change validation presented in Figure 8, it must be kept in mind that the predicted values can vary by as much as 9%.

Summary and Conclusions

A fully coupled model for multiphase transport and large deformation during microwave puffing of a hygroscopic porous material was formulated, solved using a finite element based software, and validated using experimental measurements. A comprehensive understanding of the different transient phenomena during rapid heating such as evaporation/condensation, pressure development, deformation and their relationships to transport and solid mechanics parameters was developed. Often drawbacks of such complex models are the availability of accurate input parameters. To address this issue, detailed uncertainty analysis was carried out. Such a detailed model is essential to understand a complex process such as puffing and has not been implemented earlier.

The major conclusions from the work are summarized as follows. (1) The model accurately predicts the temperatures, moisture and volume change during the puffing process as measured in this work and also reported earlier by others. (2) Very high temperatures are required to generate pressures needed to puff the material. The process may not be successful unless carried out using an intensive heating source such as microwaves. (3) Although pressures increase because of intensive microwave heating, they remain bounded because of a complex feedback mechanism that includes change in porosity and permeability of the material with puffing time that tends to decrease the pressure. (4) Moisture loss was found to be largely independent of the change in input parameters such as bulk modulus and liquid and gas permeabilities. (5) Uncertainty in the choice of permeability values affects the volume change more than the uncertainty in the bulk modulus value chosen.

Acknowledgments

This project was supported by National Research Initiative Grant number 2008-35503-18657 from the USDA Cooperative State Research, Education, and Extension Service Competitive Grants program. The authors also acknowledge the general discussions regarding solid mechanics models over the years with Prof. Subrata Mukherjee (Professor) and Haolin Zhu (Graduate student) from the Department of Theoretical and Applied Mechanics (Cornell University).

Notation

c = concentration, kg m^{-3}
c_p = specific heat capacity, J kg^{-1} K^{-1}
C = molar density, kmol m^{-3}
$D_{eff,\,g}$ = effective gas diffusivity, m^2 s^{-1}
D = capillary diffusivity, m^2 s^{-1}
$\mathbf{E}$ = Green–Lagrange strain tensor
$\mathbf{F}$ = deformation gradient tensor
G = shear modulus, Pa
h = heat transfer coefficient, W m^{-2} K^{-1}
h_m = mass transfer coefficient of vapor, m s^{-1}
I = volumetric evaporation rate, kg m^{-3} s^{-1}
j = total mass flux, kg m^{-2} s^{-1}
J = Jacobian of deformation gradient tensor, Pa
k^{th} = thermal conductivity, W m^{-1} K^{-1}
k = intrinsic permeability, m^2
k_r = relative permeability
K = bulk modulus, Pa
K_{evap} = nonequilibrium evaporation constant
m = overall mass fraction
M = moisture content, db
M_a, M_v = molecular weight of air and vapor
n = normal direction
P, p = total pressure and partial pressure, respectively, Pa
q = heat flux, W m^{-2}
Q_{mic} = microwave source term, J m^{-3} s^{-1}
R = universal gas constant, J k mol^{-1} K^{-1}
S = saturation
$\mathbf{S}$ = second Piola Kirchhoff stress tensor, Pa
t = time, s
T = temperature, °C
$\mathbf{v}$ = velocity, m s^{-1}
V = volume, m^3
W = stored energy function, Pa
x, y, z = coordinates (Eulerian frame), m
X, Y, Z = coordinates (Lagrangian frame), m

Greek letters

ρ = density, kg m^{-3}
λ = latent heat of vaporization, J kg^{-1}
ω_a, ω_v = mass fraction of air and vapor with respect to total gas
ϕ = porosity
μ = dynamic viscosity, Pa s
σ = Cauchy stress tensor, Pa

Literature Cited

1. Payne FA, Taraba JL, Saputra D. Review of puffing processes for expansion of biological products. *J Food Eng*. 1989;10(3):183–197.
2. McAlister RE. Microwave puffing of cereal grain and products made therefrom. U.S. Patent 3,682,651, 1972.
3. Krysiak DLM, Allen PE, Kirihara TT. Laminated multi-layered cereal products and methods of preparation. U.S. Patent 6,746,707, 2004.
4. Varnalis AI, Brennan JG, MacDougall DB. Proposed mechanism of high-temperature puffing of potato. Part I. The influence of blanching and drying conditions on the volume of puffed cubes. *J Food Eng*. 2001;48(4):361–367.
5. Liang S, Yin JY, Xue SF. The ALE method for oil/water two-phase flow in deforming porous media. *J Can Petroleum Technol*. 2009;48(4):72–77.
6. Lewis RW, Schrefler BA. *The Finite Element Method in the Deformation and Consolidation of Porous Media*, West Sussex, England: Wiley, 1987.
7. Choi JY, Tanenbaum BS, Milner TE, Dao XV, Nelson JS, Sobol EN, Wong RJF. Thermal, mechanical, optical, and morphologic changes in bovine nucleus pulposus induced by Nd : YAG (lambda = 1.32 mu m) laser irradiation. *Lasers Surg Med*. 2001;28(3):248–254.
8. Wu PJ, Schwartzberg HG. Popping behavior and zein coating of popcorn. *Cereal Chem*. 1992;69(5):567–573.

9. Chandrasekhar PR, Chattopadhyay PK. Rice puffing in relation to its varietal characteristics and processing conditions. *J of Food Process Eng*. 1991;14(4):261–277.
10. Hoke K, Housova J, Houska M. Optimum conditions of rice puffing. *Czech J of Food Sci*. 2005;23(1):1–11.
11. Saputra D, Payne FA, Cornelius PL. Puffing dehydrated green bell peppers with carbon dioxide. *Trans ASAE*. 1991;34(2):475–480.
12. Nath A, Chattopadhyay PK. Effect of process parameters and soy flour concentration on quality attributes and microstructural changes in ready-to-eat potato-so snack using high-temperature short time air puffing. *LWT—Food Sci Technol*. 2008;41(4):707–715.
13. Antonio GC, Alves DG, Azoubel PM, Murr FEX, Park KJ. Influence of osmotic dehydration and high temperature short time processes on dried sweet potato (Ipomoea batatas Lam.). *J Food Eng*. 2008;84(3):375–382.
14. Mariotti M, Alamprese C, Pagani MA, Lucisano M. Effect of puffing on ultrastructure and physical characteristics of cereal grains and flours. *J Cereal Sci*. 2006;43(1):47–56.
15. Tabeidie Z, Payne FA, Cornelius PL. Puffing potato pieces with CO_2. *Trans ASABE*. 1992;35(6):1935–1940.
16. Zapotoczny P, Markowski M, Majewska K, Ratajski A, Konopko H. Effect of temperature on the physical, functional, and mechanical characteristics of hot-air-puffed amaranth seeds. *J Food Eng*. 2006;76(4):469–476.
17. Schwartzberg HG, Wu JPC, Nussinovitch A, Mugerwa J. Modelling deformation and flow during vapor-induced puffing. *J Food Eng*. 1995;25(3):329–372.
18. Chiotellis E, Campbell GM. Proving of bread dough I—modelling the evolution of the bubble size distribution. *Food Bioprod Process*. 2003;81(C3):194–206.
19. Fan JT, Mitchell JR, Blanshard JMV. A model for the oven rise of dough during baking. *J Food Eng*. 1999;41(2):69–77.
20. Alavi SH, Rizvi SSH, Harriott P. Process dynamics of starch-based microcellular foams produced by supercritical fluid extrusion. I: model development. *Food Res Int*. 2003;36(4):309–319.
21. Wang LJ, Ganjyal GM, Jones DD, Weller CL, Hanna MA. Modeling of bubble growth dynamics and nonisothermal expansion in starch-based foams during extrusion. *Adv in Polym Technol*. 2005;24(1):29–45.
22. Halder A, Dhall A, Datta AK. An improved, easily implementable, porous media based model for deep-fat frying—Part I: Model development and input parameters. *Food and Bioprod Process*. 2007;85(C3):209–219.
23. Ni H, Datta AK, Torrance KE. Moisture transport in intensive microwave heating of biomaterials: a multiphase porous media model. *Int J Heat Mass Transfer*. 1999;42(8):1501–1512.
24. Rakesh V, Datta AK, Walton JH, McCarthy KL, McCarthy MJ. Microwave combination heating: coupled electromagnetics—multiphase porous media modeling and MRI experimentation. *AIChE J*. 2012;58(4):1262–1278. DOI: 10.1002/aic.12659.
25. Yamsaengsung R, Moreira RG. Modeling the transport phenomena and structural changes during deep fat frying—Part 1: model development. *J Food Eng*. 2002;53(1):1–10.
26. Turner IW, Perre P. Vacuum drying of wood with radiative heating: II. comparison between theory and experiment. *AIChE J*. 2004;50(1):108–118.
27. Shi X, Datta AK, Mukherjee Y. Thermal stresses from large volumetric expansion during freezing of biomaterials. *J Biomech Eng—Trans ASME*. 1998;120(6):720–726.
28. Baek S, Wells PB, Rajagopal KR, Humphrey JD. Heat-induced changes in the finite strain viscoelastic behavior of a collaagenous tissue. *J Biomech Eng—Trans ASME*. 2005;127(4):580–586.
29. Niamnuy C, Devahastin S, Soponronnarit S, Raghavan GSV. Modeling coupled transport phenomena and mechanical deformation of shrimp during drying in a jet spouted bed dryer. *Chem Eng Sci*. 2008;63(22):5503–5512.
30. Ressing H, Ressing M, Durance T. Modeling the mechanisms of dough puffing during vacuum microwave drying using the finite element method. *J Food Eng*. 2007;82(4):498–508.
31. Minkoff SE, Kridler NM. A comparison of adaptive time stepping methods for coupled flow and deformation modeling. *Appli Math Modell*. 2006;30(9):993–1009.
32. Itaya Y, Kobayashi T, Hayakawa KI. 3-Dimensional heat and moisture transfer with viscoelastic strain–stress formation in composite food during drying. *Int J Heat Mass Transfer*. 1995;38(7):1173–1185.
33. Irudayaraj J, Haghighi K. Stress-analysis of viscoelastic materials during drying .1. Theory and finite-element formulation. *Drying Technol*. 1993;11(5):901–927.
34. Perre P, Turner IW, Passard J. 2-D solution for drying with internal vaporization of anisotropic media. *AIChE J*. 1999;45(1):13–26.
35. Yang DQ, Rahardjo H, Leong EC, Choa V. Coupled model for heat, moisture, air flow, and deformation problems in unsaturated soils. *J Eng Mech-ASCE*. 1998;124(12):1331–1338.
36. Mayor L, Sereno AM. Modelling shrinkage during convective drying of food materials: a review. *J Food Eng*. 2004;61(3):373–386.
37. Di Y, Yang J, Sato T. An operator-split ALE model for large deformation analysis of geomaterials. *Int J Numer Anal Methods Geomech*. 2007;31(12):1375–1399.
38. Bollada PC. Expansion of elastic bodies with application in the bread industry. *Math Comput Modell*. 2008;48(7–8):1055–1067.
39. Khalili N. Two-phase fluid flow through fractured porous media with deformable matrix. *Water Res Res*. 2008; 44.
40. Chao L, Borja RI, Regueiro RA. Dynamics of porous media at finite strain. *Comput Methods Appl Mech Eng*. 2004;193(36–38):3837–3870.
41. Zhang J, Datta AK, Mukherjee S. Transport processes and large deformation during baking of bread. *AIChE J*. 2005;51(9):2569–2580.
42. Biot MA. *Mechanics of Incremental Deformations*, New York, NY: Wiley, 1965.
43. Coussy O. *Poromechanics*, West Sussex, England: Wiley, 2004.
44. Belytschko T, Liu WK, Moran B. *Nonlinear Finite Elements for Continua and Structures*, West Sussex, England: Wiley, 2001.
45. Donea J, Huerta A, Ponthot JP, Rodríguez-Ferran. *Arbitrary Lagrangian–Eulerian methods*. In: Stein E, Borst RD, Hughes TJR, editors. *Encyclopedia of Computational Mechanics*, Vol. 1. West Sussex, England: Wiley, 2004.
46. Bear J. *Dynamics of Fluids in Porous Media*, New York, NY: Dover Publications Inc, 1972.
47. Datta AK. Porous media approaches to studying simultaneous heat and mass transfer in food processes. I: Problem formulations. *J Food Eng*. 2007;80(1):80–95.
48. Ni H, Datta AK. Heat and moisture transfer in baking of potato slabs. *Drying Technol*. 1999;17(10):2069–2092.
49. Choi Y, Okos MR. *Thermal properties of liquid foods review*. In: Okos MR, editor. *Physical and Chemical Properties of Food*, St Joseph, MI: American Society of Agricultural Engineers, 1986:35–77.
50. Ratti C, Crapiste GH, Rotstein E. A new water sorption equilibrium expression for solid foods based on thermodynamic considerations. *J Food Sci*. 1989;54(3):738–747.
51. Jarvis MC, Mackenzie E, Duncan HJ. The Textural Analysis of cooked potato. 2. Swelling pressure of starch during gelatinization. *Potato Res*. 1992;35(2):93–102.
52. Blaszczak W, Sadowska J, Fornal J, Vacek J, Flis B, Zagorski-Ostoja W. Influence of cooking and microwave heating on microstructure and mechanical properties of transgenic potatoes. *Nahrung-Food*. 2004;48(3):169–176.
53. Alvarez MD, Canet W. Kinetics of thermal softening of potato tissue heated by different methods. *Euro Food Res Technol*. 2001;212(4):454–464.
54. Ni H. Multiphase moisture transport in porous media under intensive microwave heating. PhD Thesis. Cornell University, 1997.
55. Shames IH, Pitarresi JM. *Introduction to Solid Mechanics*, 3rd ed. Upper Saddle River, NJ: Prentice Hall, 1999.
56. Simo JC, Hughes TJR. *Computational Inelasticity*, New York, NY: Springer-Verlag Inc, 1998.
57. Solomon WK, Jindal VK. Relationship between texture of raw and cooked potatoes. *J Text Stud*. 2005;36(5–6):589–604.
58. Krokida MK, Maroulis ZB. The effect of drying methods on viscoelastic behaviour of dehydrated fruits and vegetables. *Int J Food Sci Technol*. 2000;35(4):391–400.
59. Buffler CR. *Microwave Cooking and Processing: Engineering Fundamentals for the Food Scientist*, New York: Van Nostrand Reinhold, 1993: 4–31, 157–159
60. Zhang H, Datta AK. Microwave power absorption in single- and multiple-item foods. *Food Bioprod Process*. 2003;81(C3):257–265.
61. AACC. *Approved methods of the AACC. Method 74–09*, St. Paul, MN: American Association of Cereal Chemists, 1988.
62. Varnalis AI, Brennan JG, MacDougall DB, Gilmour SG. Optimisation of high temperature puffing of potato cubes using response surface methodology. *J Food Eng*. 2004;61(2):153–163.

63. Bell LN, Labuza TP. *Practical Aspects of Moisture Sorption Isotherm Measurement and Use*, 2nd Ed. Egan, MN: AACC Egan Press, 2000.
64. Rizvi SSH. *Thermodynamic properties of foods in dehydration*. In: Rao MA, Rizvi SSH, Datta AK editors. *Engineering Properties of Foods*, 3rd Ed. Boca Raton, FL: CRC Press, 2005.
65. Datta AK. Hydraulic permeability of food tissues. *Int J Food Properties*. 2006;9(4):767–780.
66. Rabin Y. A general model for the propagation of uncertainty in measurements into heat transfer simulations and its application to cryosurgery. *Cryobiology*. 2003;46(2):109–120.
67. Holman JP. *Experimental Methods for Engineers*, 7th Ed. New York: McGraw-Hill, 2001.

Manuscript received Aug. 2, 2011, and revision received Feb. 26, 2012.